DESY 01-116
LUNFD6/(NFFL–7204) 2001
hep-ph/0204269

arXiv:hep-ph/0204269v1 23 Apr 2002

Massive $c\bar{c}g$ - Calculation in Diffractive DIS and Diffractive D^* - Production at HERA

J. Bartels[1], H. Jung[2], A. Kyrieleis[1]
[1]*II. Institut für Theoretische Physik, Universität Hamburg, Germany* *
[2]*Department of Physics, Lund University, Sweden*

Abstract: We calculate the cross section for $c\bar{c}g$-production in diffractive DIS with finite quark masses at zero momentum transfer t. The calculation is done in the leading $\log(1/x_{\mathbb{P}})$ approximation and is valid in the region of high diffractive masses M (small β). We apply our cross section formula including both $c\bar{c}$- and $c\bar{c}g$ in a Monte Carlo simulation to diffractive $D^{*\pm}$ meson production at HERA. We compare our predictions to results of H1 using three parameterizations for the unintegrated gluon density.

1 Introduction

In the process of diffractive deep inelastic scattering, $\gamma^* + p \to p + X$, one can separate perturbative and non-perturbative contributions by filtering out particular diffractive final states. Examples of diffractive states which are perturbatively calculable are longitudinal vector particles or final states which consist of hard jets (and no soft remnant). In the latter case the hard scale which allows the use of pQCD is provided by the large transverse momenta of the jets, and the Pomeron exchange is modeled by the unintegrated gluon density. Another particularly interesting example is diffractive charm production, since the charm quark mass justifies pQCD, even for not so large transverse momenta of the outgoing quarks and gluons. Calculations for the diffractive production of massless open $q\bar{q}$ states and of massless $q\bar{q}g$ states have been reported in [1, 2, 3] and in [4], respectively, and a comparison of diffractive two-jet and three-jet events observed at HERA with these calculations has been presented in [5]. Final states with finite quark masses have been calculated, so far, only for $q\bar{q}$ production [6] which is expected to be the dominant final state in the region of small diffractive masses (large β). However, as there are recent measurements of diffractive $D^{*\pm}$ - production from the H1 [7] and ZEUS [8] collaborations at HERA, which extend into the small-β-region, gluon radiation can certainly not be neglected, and a full perturbative calculation of $q\bar{q}g$ is needed.

In this article we report on a calculation of massive $q\bar{q}g$-production in diffractive deep inelastic scattering, and we present a comparison of our cross section formula with the measurements of H1 [7].

*Supported by the TMR Network "QCD and Deep Structure of Elementary Particles"

2 Calculation of massive $q\bar{q}g$ production

We will follow the study of massless $q\bar{q}g$-production presented in [4]. In particular, we again work in the leading-log M^2 approximation, which limits the applicability of our results to the small β-region. Fig. 1 shows the notations of the process. As in [4] we restrict ourselves to zero momentum transfer, $t = r^2 = 0$. As usually, Q^2 denotes the virtuality of the photon, $\sqrt{W^2}$ the energy of the photon proton system, M the mass of the diffractive system, and $x = Q^2/(Q^2 + W^2)$, $y = pq/pl$ are the Bjorken scaling variables (with l being the momentum of the incoming electron). The variable β is defined as $\beta = Q^2/(Q^2 + M^2)$, and it is convenient to introduce the momentum fraction of the Pomeron by $x_{\mathbb{P}} = (Q^2 + M^2)/(Q^2 + W^2)$.

We restrict our calculation to the region (leading-log M^2 approximation):

$$Q^2 \ll M^2 \ll W^2. \tag{1}$$

We use Sudakov variables $k_i = \alpha_i q' + \beta_i p + k_{i\,t}$ (with $q' = q + xp$, $k_{i\,t}^2 = -\mathbf{k}_i^2$), and we express

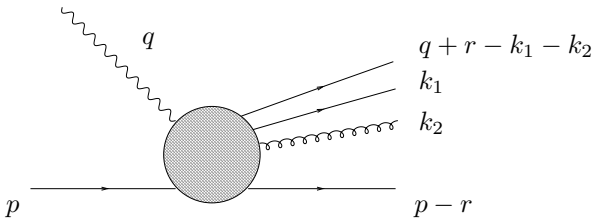

Figure 1: Kinematics of diffractive $q\bar{q}g$ production

the phase space in terms of y, Q^2, M^2, m^2, t, $\mathbf{k}_1^2$, $\mathbf{k}_2^2$ with $m^2 = m_{qq}^2 + \mathbf{k}_2^2$ (m_{qq} denotes the invariant mass of the $q\bar{q}$-subsystem). We obtain the following result:

$$\frac{d\sigma_D^{e^-p}}{dydQ^2dM^2dm^2d^2\mathbf{k}_1d^2\mathbf{k}_2dt}_{|t=0} = \frac{\alpha_{em}}{yQ^2\pi}\cdot$$

$$\cdot\left[\frac{1+(1-y)^2}{2}\frac{d\sigma_{D,T+}^{\gamma^*p}}{dM^2dm^2d^2\mathbf{k}_1d^2\mathbf{k}_2dt_{|t=0}} - 2(1-y)\frac{d\sigma_{D,T-}^{\gamma^*p}}{dM^2dm^2d^2\mathbf{k}_1d^2\mathbf{k}_2dt_{|t=0}}\right.$$
$$\left. + (1-y)\frac{d\sigma_{D,L}^{\gamma^*p}}{dM^2dm^2d^2\mathbf{k}_1d^2\mathbf{k}_2dt_{|t=0}} + (2-y)\sqrt{1-y}\frac{d\sigma_{D,I}^{\gamma^*p}}{dM^2dm^2d^2\mathbf{k}_1d^2\mathbf{k}_2dt_{|t=0}}\right], \tag{2}$$

The differential cross sections of $\gamma^*p \to ccg + p$ are given by:

$$\frac{d\sigma_{D,T+}^{\gamma^*p}}{dM^2dm^2d^2\mathbf{k}_1d^2\mathbf{k}_2dt_{|t=0}} = \frac{9}{128\pi}\frac{1}{\sqrt{S}(M^2-m^2)m^2}e_c^2\alpha_{em}\alpha_s^3\alpha_1(1-\alpha_1)\cdot$$
$$\cdot\left[\left(\alpha_1^2+(1-\alpha_1)^2\right)M_{il}M'_{il} + m_q^2M_lM'_l\right] \tag{3}$$

$$\frac{d\sigma_{D,T-}^{\gamma^*p}}{dM^2dm^2d^2\mathbf{k}_1d^2\mathbf{k}_2dt_{|t=0}} = \frac{9}{128\pi}\frac{1}{\sqrt{S}(M^2-m^2)m^2}e_c^2\alpha_{em}\alpha_s^3\alpha_1^2(1-\alpha_1)^2\cdot$$
$$\cdot\left[M_{1l}M'_{1l} - M_{2l}M'_{2l}\right] \tag{4}$$

$$\frac{d\sigma_{D,L}^{\gamma^* p}}{dM^2 dm^2 d^2\mathbf{k}_1 d^2\mathbf{k}_2 dt_{|t=0}} = \frac{9}{128\pi}\frac{1}{\sqrt{S}(M^2-m^2)m^2} e_c^2 \alpha_{em}\alpha_s^3 4\alpha_1^3(1-\alpha_1)^3 Q^2 M_l M_l' \quad (5)$$

$$\frac{d\sigma_{D,I}^{\gamma^* p}}{dM^2 dm^2 d^2\mathbf{k}_1 d^2\mathbf{k}_2 dt_{|t=0}} = \frac{9}{128\pi}\frac{1}{\sqrt{S}(M^2-m^2)m^2} e_c^2 \alpha_{em}\alpha_s^3\alpha_1^2(1-\alpha_1)^2(1-2\alpha_1)\cdot \cdot\sqrt{Q^2}\left[M_{1l}M_l' + M_l M_{1l}'\right] \quad (6)$$

with

$$S = \left(1 + \frac{\mathbf{k}_1^2}{m^2} - \frac{(\mathbf{k}_1+\mathbf{k}_2)^2}{m^2}\right)^2 - 4\frac{(\mathbf{k}_1^2+m_q^2)}{m^2}, \quad (7)$$

$$M_{il} = \int \frac{d^2\mathbf{l}}{\pi \mathbf{l}^2}\mathcal{F}(x_{\mathbb{P}}, \mathbf{l}^2) T_{il}, \quad (8)$$

and

$$T_{il} = \left(\frac{\mathbf{l}+\mathbf{k}_1+\mathbf{k}_2}{D(\mathbf{l}+\mathbf{k}_1+\mathbf{k}_2)} + \frac{\mathbf{k}_1+\mathbf{k}_2}{D(\mathbf{k}_1+\mathbf{k}_2)} - \frac{\mathbf{k}_1-\mathbf{l}}{D(\mathbf{k}_1-\mathbf{l})} - \frac{\mathbf{k}_1}{D(\mathbf{k}_1)}\right)_i \left(\frac{\mathbf{l}+\mathbf{k}_2}{(\mathbf{l}+\mathbf{k}_2)^2} - \frac{\mathbf{k}_2}{\mathbf{k}_2^2}\right)_l + (\mathbf{l}\to -\mathbf{l}) \quad (9)$$

$$T_{l} = \left(\frac{1}{D(\mathbf{l}+\mathbf{k}_1+\mathbf{k}_2)} + \frac{1}{D(\mathbf{k}_1+\mathbf{k}_2)} - \frac{1}{D(\mathbf{k}_1-\mathbf{l})} - \frac{1}{D(\mathbf{k}_1)}\right) \left(\frac{\mathbf{l}+\mathbf{k}_2}{(\mathbf{l}+\mathbf{k}_2)^2} - \frac{\mathbf{k}_2}{\mathbf{k}_2^2}\right)_l + (\mathbf{l}\to -\mathbf{l}). \quad (10)$$

Here

$$D(\mathbf{k}) = \alpha_1(1-\alpha_1)Q^2 + \mathbf{k}^2 + m_q^2, \quad (11)$$

and the function $\mathcal{F}$ denotes the unintegrated (forward) gluon density[1] which is connected with the usual gluon density $g(x,Q^2)$ through:

$$\int_0^{Q^2} d\mathbf{l}^2 \mathcal{F}(x,\mathbf{l}^2) \simeq x g(x,Q^2). \quad (12)$$

The $\simeq$ sign in the above equation indicates that the relation is valid for large Q^2. Strictly speaking, the kinematics of diffractive $q\bar{q}g$ production requires the nonforward (skewed) gluon density. However, our cross section formula has been derived in the leading-$\ln W^2$, leading-$\ln M^2$ approximation, and the use of the gluon density in (12) is valid only in the double logarithmic approximation where skewedness is negligeable.

The parameter α_1 is determined by the on-shell conditions for the final state particles:

$$\alpha_1 = \frac{1}{2}\left[1 + \frac{\mathbf{k}_1^2}{m^2} - \frac{(\mathbf{k}_1+\mathbf{k}_2)^2}{m^2} \pm \sqrt{S}\right], \quad (13)$$

[1]Note that different definitions for $\mathcal{F}$ exist, here we use $\mathcal{F}$ as defined in eq.(8).

and it varies between 0 and 1. The values of the momenta $\mathbf{k}_1$, $\mathbf{k}_2$ and of m^2 determine the sign in eq.(13). The validity of our cross section formula is restricted to the kinematic region where the gluon transverse momentum $\mathbf{k}_2$ is not small.

The quark mass m_q enters the calculations in two places. First, the phase space of the diffractive system (and so the parameter α_1 and the function S) depend upon the quark mass via the on-shell conditions for the outgoing particles. Secondly, the propagators of the internal fermion lines are modified by a nonzero quark mass which leads to changes in the matrix-elements. Apart from the function $D(\mathbf{k})$, eq.(11), which enters in all four $\gamma^* p$ - cross sections, an additional term containing the quark mass emerges in $d\sigma^{\gamma^* p}_{D,T+}$ (eq.(3)).

3 Comparison with measurements

Compared to other charmed particles, $D^{*\pm}$ mesons are easy to reconstruct which makes them attractive objects for testing diffractive charm production. $D^{*\pm}$ mesons are identified via the decay channel

$$D^{*+} \to D^0 \pi^+_{slow} \to (K^- \pi^+)\pi^+_{slow} \qquad \text{(and c.c.)},$$

which has a branching ratio of 2.63% [9]. In the following comparison we concentrate on a comparison with the measurement of the H1 collaboration [7], who has analyzed data collected throughout the years 1995-1997. The amount of data is still quite poor due to the small branching ratio of the D^* meson, but higher statistics will come from new data.

We have implemented the cross section formulae for diffractive massive $c\bar{c}$ production [6] and from our expression eq.(2-6) for the massive $q\bar{q}g$ production into the Monte Carlo generator RAPGAP [10, 11], which includes full hadronization according to the Lund string model as implemented in JETSET/PYTHIA [12, 13]. We have used a fixed strong coupling constant $\alpha_s = 0.25$, and a charm quark mass of $m_q = 1.5$ GeV. The transition of the charm quark to the D^* meson is performed via the Lund heavy quark fragmentation function. Since the experimental measurement does not separate the charge of the D^* meson, we have added the cross sections of both charged D^* mesons.

Events generated with RAPGAP are selected within the same kinematic region as in the measurement of H1 [7], using electron and proton momenta (in the HERA system) of 27.6 GeV and 820 GeV, respectively, and:

$$\begin{aligned} 0.05 \quad &\leq y \quad &&\leq 0.7 \\ 2 \quad &\leq Q^2 \quad &&\leq 100 \text{ GeV}^2 \\ &x_{\mathbb{P}} \quad &&< 0.04 \\ &|t| \quad &&< 1 \text{ GeV}^2 \end{aligned} \tag{14}$$

As the measured cross section is integrated over t for $|t| \leq 1$ GeV^2, we have multiplied our cross section formulas (eq.(2-6)), valid for $|t| = 0$, with a phenomenologically motivated t distribution of the form:

$$f^2(t) = \left(\frac{4 - 2.8t}{4 - t} \frac{1}{\left(1 - \frac{t}{0.7}\right)^2} \right)^2 \tag{15}$$

The D^* mesons are experimentally detected in the range:

$$\begin{aligned} |\eta(D^{*\pm})| &< 1.5 \\ p_T(D^{*\pm}) &> 2 \text{ GeV} \end{aligned} \tag{16}$$

with the pseudo-rapidity $\eta = -\log\tan(\theta/2)$ and the transverse momentum p_T of the D^* meson measured in the ep laboratory system.

As can be seen from eqs.(9,10), there is a potential divergency, if the transverse momentum of the final state gluon $\mathbf{k}_2^2$ approaches zero. In order to avoid the non-perturbative region, we

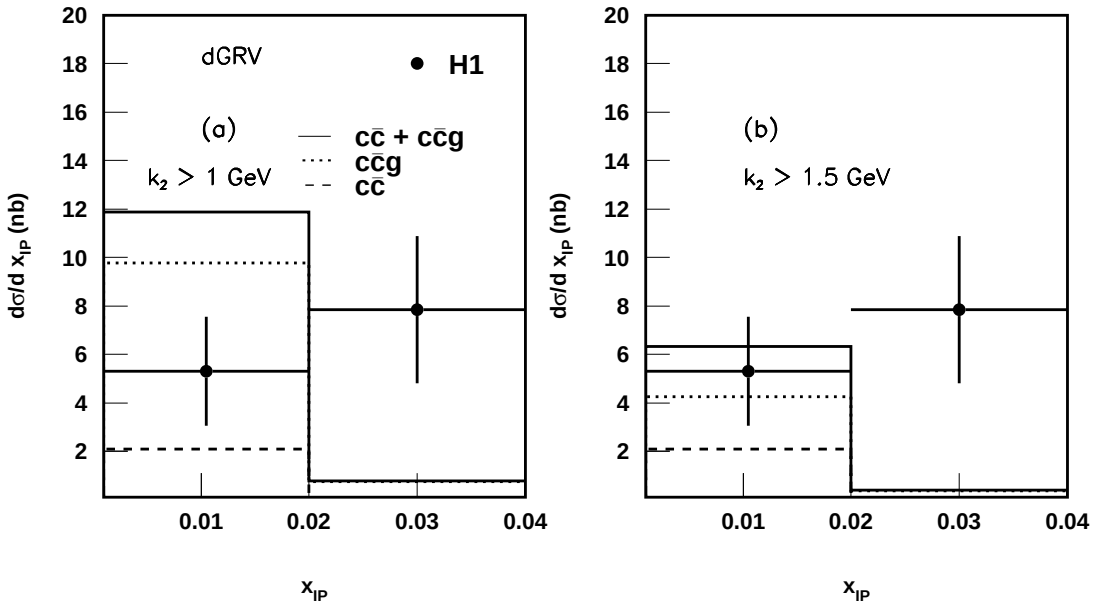

Figure 2: The cross section $d\sigma/d\log_{10} x_{\mathbb{P}}$ for diffractive D^* production within the kinematic range specified in the text. The point are the measured cross section from H1 [7]. The prediction obtained with $\mathbf{k}_{cut} = 1$ (1.5) GeV is shown in a (b). The dashed (dotted) line shows the $c\bar{c}$ ($c\bar{c}g$) contribution alone and the solid line is the sum of both. The $dGRV$ unintegrated gluon density is used, with $\mathbf{l}^2_{min} = 0.4\text{GeV}^2$.

impose a lower cutoff $\mathbf{k}^2_{2cut}$ on the gluon transverse momentum. In our calculations we have considered $\mathbf{k}_{2cut} = 1$ GeV and $\mathbf{k}_{2cut} = 1.5$ GeV. For the unintegrated gluon density, which enters in eq.(8), we have used three different approaches: the derivative of the NLO GRV [14] gluon density $dGRV$, the unintegrated gluon density $\mathcal{F}(x, \mathbf{l}^2)$ obtained in the saturation model of Golec-Biernat and Wüsthoff [15] GBW, and the CCFM [16, 17, 18, 19] unintegrated gluon density $\mathcal{A}(x, \mathbf{l}^2, \bar{q}^2)$ JS of [20, 21], where $\bar{q}$ defines the evolution scale, related to the maximum allowed angle of any emission in the angular ordering approach.

The unintegrated gluon density can be obtained from the integrated gluon density, if in

eq.(12) the $\simeq$ sign is replaced by an equality sign:

$$\mathcal{F}(x,\mathbf{l}^2) = \left.\frac{\partial\, xg(x,\mu^2)}{\partial\,\mu^2}\right|_{\mu^2=\mathbf{l}^2} \tag{17}$$

Here we use for $xg(x,\mu^2)$ the NLO GRV [14] gluon density, since it is the only integrated gluon density available, starting at a low value of $Q_0^2 = 0.4$ GeV^2. Due to the finite Q_0 in any of the available integrated gluon densities, a lower integration limit $\mathbf{l}^2_{min} \simeq Q_0^2$ in eq.(8) is introduced. Variation of this parameter mainly affects the normalization of the cross sections. For example, when $\mathbf{l}^2_{min}$ is decreased from 1 to 0.5 GeV^2, the $x_{\mathbb{P}}$-distribution at $\mathbf{k}_{2cut} = 1$ GeV roughly doubles in the whole $x_{\mathbb{P}}$ range. We have chosen to set $\mathbf{l}^2_{min}$ as small as it is compatible with the definition of the integrated gluon density, so $\mathbf{l}^2_{min} = 0.4$ GeV^2 for *dGRV*. The other two unintegrated gluon densities, *GBW* and *JS*, are defined also for the very small $\mathbf{l}^2$ region, and therefore no cut needs to be applied there. In the numerical treatment of the $c\bar{c}$ production cross section neither $\mathbf{k}^2_{2cut}$ nor $\mathbf{l}^2_{min}$ are needed.

In Fig. 2 we show the effect of changing the cut $\mathbf{k}^2_{cut}$ on the differential cross section $d\sigma/dlog_{10}x_{\mathbb{P}}$, for diffractive D^* meson production in the kinematic region specified above and compare our prediction to the measurement of H1 [7]. Also shown in Fig. 2 are the individual contributions of $c\bar{c}$ (dashed histogram) and $c\bar{c}g$ (dotted histogram). One clearly sees the reduction of the $c\bar{c}g$ contribution when the cutoff in $\mathbf{k}_{cut}$ is increased. Since our calculation is valid for small $x_{\mathbb{P}}$, we focus only on agreement in the low $x_{\mathbb{P}}$ region. A cutoff value of $\mathbf{k}^2_{cut} = 1.5$ GeV^2 seems to be a reasonable choice which we will keep independently of the choice of the unintegrated gluon density. With this cut the computed cross section in the lower $x_{\mathbb{P}}$ bin agrees well with the data. In the upper $x_{\mathbb{P}}$ bin, however, the theoretical curve is by a factor of about 10 smaller than the data point (ignoring the large error on the measurement). In this $x_{\mathbb{P}}$-region it is expected that, apart from Pomeron exchange (which, in our model, is the 2-gluon exchange) secondary exchanges have to be included: in a perturbative description such an exchange corresponds to $q\bar{q}$-exchange. Since such a contribution has not yet been included into our calculation, it is not surprising that the two-gluon model undershoots the data.

In Fig. 3*a* we compare our prediction of the cross section for diffractive D^* production as a function of $\log_{10}\beta$ with the measurement of H1 (it is understood, that all other variables, in particular $x_{\mathbb{P}}$, are integrated over). We also show the individual contributions of $c\bar{c}$ (dashed histogram) and $c\bar{c}g$ (dotted histogram). Clearly, the $c\bar{c}g$ is badly needed in order to get closer to the data than with $c\bar{c}$ alone. The measured cross section is slowly rising with decreasing $\log_{10}\beta$. The theoretical curve does not quite follow this rise, the reason for this is the correlation between β and $x_{\mathbb{P}}$: small β values require large diffractive masses M, which due to the kinematic restrictions in the analysis, are predominantly produced at large $x_{\mathbb{P}}$. As argued above the large $x_{\mathbb{P}}$-region needs secondary exchange which in our approach is not yet included. For illustration, we show in Fig. 3*b* the cross section for diffractive D^* production $d\sigma/d\beta$. We observe that the strong drop in cross section at small β, as seen in Fig. 3*a* is a consequence of plotting $d\sigma/d\log_{10}\beta$ instead of $d\sigma/d\beta$. From Fig. 3*b* we see that the theoretical curve increases towards low β, and only at $\beta < 0.01$ is decreasing, which again is a consequence of kinematic correlations. If the double differential cross section $d^2\sigma/d\beta dx_{\mathbb{P}}$ is considered, our prediction shows the expected rise towards small β at fixed $x_{\mathbb{P}}$. The shape of the theoretical curves as a function of β is almost independent of the choice of the cutoffs $\mathbf{l}^2_{min}$ and $\mathbf{k}_{cut}$, as they mainly affect the overall magnitude of the cross section. In the small β region, corresponding to large diffractive masses M, also the radiation of more than one gluon, such as $c\bar{c}gg$ need to be considered. Since experimentally

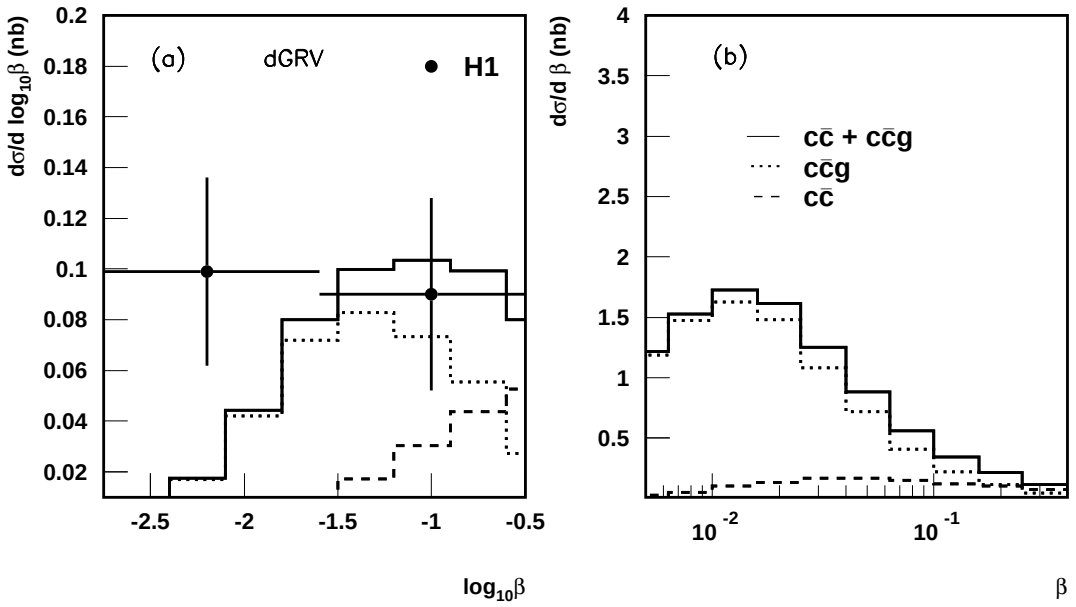

Figure 3: The differential cross section $d\sigma/d\log_{10}\beta$ for diffractive D^* production compared to the measured cross section from H1 (a). In (b) the differential cross section $d\sigma/d\beta$ is shown. In all cases we use $\mathbf{k}_{cut} = 1.5$ GeV and the $dGRV$ unintegrated gluon density. The dashed (dotted) line shows the $c\bar{c}$ ($c\bar{c}g$) contribution alone and the solid line is the sum of both.

the cross section is defined as $e + p \to e' + (D^* + X) + p_{diff}$, where in the diffractive system $M = D^* + X$, the hadronic state X is not further specified or measured, multiple soft gluon contributions might be present in the data, which have yet not been estimated consistently in the perturbative calculations.

The saturation model of K.Golec-Biernat and M.Wüsthoff [15] describes a completely different approach to estimate the unintegrated gluon density $\mathcal{F}(x, \mathbf{l}^2)$, which is needed in eq.(8). In this model the total $\gamma^* p$ cross section is described by the interaction of a $q\bar{q}$ pair (dipole) with the proton, and a particular ansatz is made for the dipole cross section. The function $\mathcal{F}(x, \mathbf{l}^2)$ has the form

$$\mathcal{F}(x, \mathbf{l}^2) = \frac{3\sigma_0}{4\pi^2\alpha_s} R_0^2(x) \mathbf{l}^2 e^{-R_0^2(x)\,\mathbf{l}^2} \quad , \qquad R_0 = \frac{1}{\mathrm{GeV}} \left(\frac{x}{x_0}\right)^{\lambda/2} , \tag{18}$$

and the three parameters of the model are determined by fitting inclusive DIS data (including charm with: $\sigma_0 = 29.12$ mb$, \lambda = 0.277,\ x_0 = 0.41\ 10^{-4}$ and $\alpha_s = 0.2$ [15]). For large $\mathbf{l}^2$, $\mathcal{F}(x, \mathbf{l}^2)$ has the meaning of the unintegrated gluon density, but for smaller $\mathbf{l}^2$ the function looses this interpretation and has to be viewed as a (model dependent) extrapolation. The ansatz eq.(18) holds for the $q\bar{q}$ color dipole cross section. The $q\bar{q}g$ system consists of a color triplet, and anti-triplet and a color octet, and one expects that the dominant configuration is

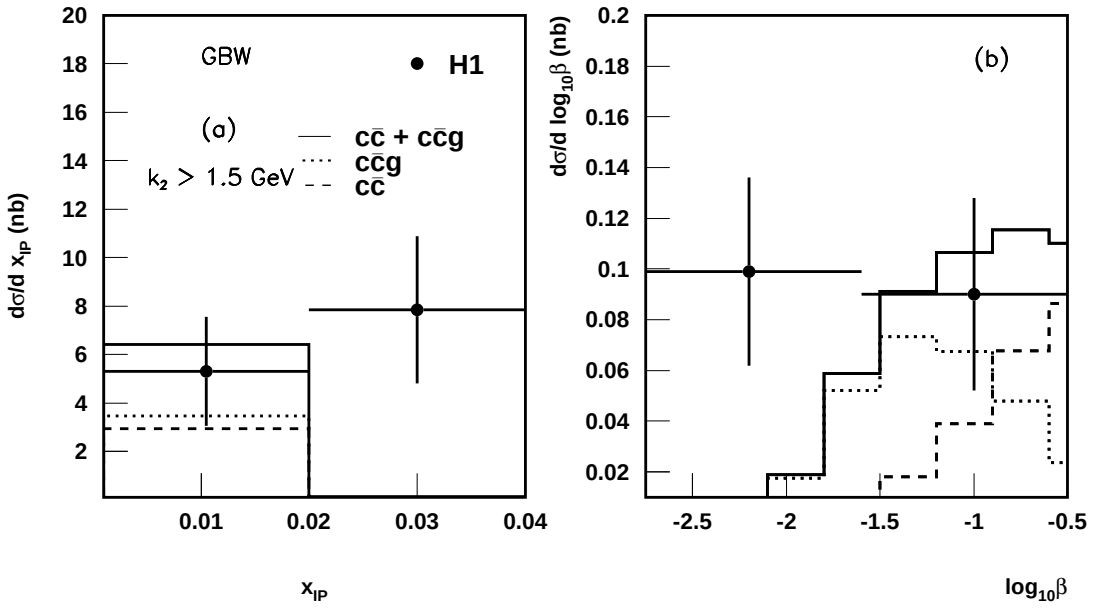

Figure 4: The differential cross section $d\sigma/d\log_{10}\beta$ for diffractive D^* production compared to the measured cross section from H1 (a). In (b) the differential cross section $d\sigma/d\beta$ is shown. In all cases we use $\mathbf{k}_{cut} = 1.5$ GeV and the GBW unintegrated gluon density from the saturation model. The dashed (dotted) line shows the $c\bar{c}$ ($c\bar{c}g$) contribution alone and the solid line is the sum of both.

a dipole consisting of two octets: in eq.(18) we therefore rescale the color charge and use:

$$\mathcal{F}(x,\mathbf{l}^2) = \frac{3\sigma_0}{2.25^2\cdot 4\pi^2\alpha_s}\, R_0^2(x)\mathbf{l}^2 e^{\frac{-R_0^2(x)}{2.25}\mathbf{l}^2} \quad . \tag{19}$$

Insertion of the ansatz (eqs.(18,19)) into eq.(12) leads to an integrand that vanishes as $\mathbf{l}^2$ goes to zero. Therefore, within this model we no longer need any lower cutoff in the $\mathbf{l}^2$ integral, and our calculation provides absolute predictions of the cross sections (note, however, that we still have the cutoff $\mathbf{k}_{cut} = 1.5$ GeV on the final state gluon). Fig. 4 shows the differential cross section $d\sigma/d\log_{10} x_{\mathbb{P}}$ calculated using eq.(18,19) compared to the measurement of H1. The calculated cross section ($c\bar{c}$+$c\bar{c}g$) is similar to that of Fig. 3, and the same discussion applies. Also the β distribution (Fig. 4b) is very similar to the previous model. Note that without the correcting color factor in the dipole cross section formula the $c\bar{c}g$ cross section would be larger by about a factor of about 1.5.

The unintegrated gluon density, based on the consistent treatment of color coherence effects, is described by the CCFM evolution equation [16, 17, 18, 19]. According to the CCFM equation, the emission of partons during the initial state cascade is allowed only in an angular-ordered region of phase space. In the large (small) x limit, the CCFM equation is equivalent to the DGLAP (BFKL) evolution equations, respectively. A solution of the CCFM equation has

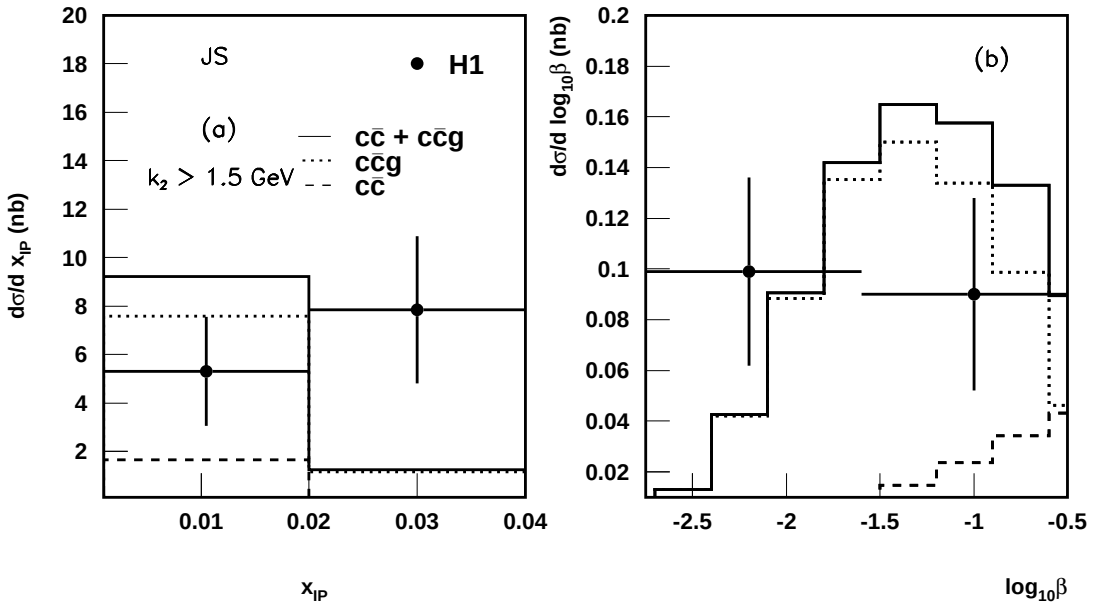

Figure 5: The differential cross section $d\sigma/d\log_{10}\beta$ for diffractive D^* production compared to the measured cross section from H1 (a). In (b) the differential cross section $d\sigma/d\beta$ is shown. In all cases we use $\mathbf{k}_{cut} = 1.5$ GeV and the CCFM based JS unintegrated gluon density. The dashed (dotted) line shows the $c\bar{c}$ ($c\bar{c}g$) contribution alone and the solid line is the sum of both.

been found, which successfully can be used to describe a bulk of measurements at HERA and the Tevatron [20, 21, 22]. However, due to the angular ordering requirement, the unintegrated gluon density $\mathcal{A}(x, \mathbf{l}^2, \bar{q}^2)$ is now also a function of the evolution scale $\bar{q}$, which is related to the maximum allowed angle. Here, this scale is set either by the $q\bar{q}$ pair, or by the final state gluon for $q\bar{q}g$:

$$\bar{q}^2 = \begin{cases} m_{q\bar{q}}^2 + \mathbf{Q}_t^2 & \text{for } q\bar{q} \\ \frac{\mathbf{k}_2^2}{1-z} & \text{for } q\bar{q}g \end{cases} \tag{20}$$

with $\mathbf{Q}_t$ being the vectorial sum of the transverse momenta of the $q\bar{q}$ pair, and $z = (Q^2 + m_{qq}^2)/(Q^2 + M^2)$. Since the explicit parameterization of $\mathcal{A}(x, \mathbf{l}^2, \bar{q}^2)$ from [20] is valid also in the very small $\mathbf{l}^2$ region, no cut on $\mathbf{l}^2$ needs to be applied for the integral in eq. (8). The results for the differential cross sections as a function of $x_{\mathbb{P}}$ and the $\log_{10}\beta$ shown in Fig. 5a and b are quite similar to those of the unintegrated gluon density from saturation model GBW and or from the derivative of the integrated gluon density $dGRV$. The main difference is the ratio of $c\bar{c}$ and $c\bar{c}g$ contribution. The enhancement of the β distribution by $c\bar{c}g$ is much stronger than in case of the two other models.

4 Conclusion

In this article we have analyzed DIS diffractive charm production (production of $D^{*\pm}$ mesons) within the perturbative two-gluon model. For the two-gluon amplitude we have used three different models: the unintegrated gluon density derived from the integrated DGLAP gluon density *dGRV*, the saturation model of Golec-Biernat and Wüsthoff *GBW*, and a CCFM-based unintegrated gluon density *JS* (the last two models are parameter-free, the first one depends upon a cutoff on the internal momentum integral). In all three cases the calculated cross sections are of the same order of magnitude as the data, and within the kinematical region where the models apply, the shapes of the cross sections are consistent with the data. Compared to an earlier attempt (with the *dGRV* gluon density) where only $c\bar{c}$ production had been included in the theoretical analysis the present analysis contains, as the new ingredient, also (massive) $c\bar{c}g$ production and leads to a considerable improvement in the agreement with experimental data.

It is encouraging to see that, for the *dGRV* gluon density, our analysis of diffractive charm production uses the same parameters as in the successful analysis of diffractive jet production and we were able to consistently describe both types of processes.

We view the use of the two-gluon model as part of a more general strategy of analyzing DIS diffraction data at HERA. In a first step one would analyze those diffractive final states which are dominated by short distances (diffractive jets or states consisting of heavy quarks): in these processes the application of the two-gluon model can be justified. In a second step, one would try to extrapolate also into kinematic regions where soft physics becomes important. In the present analysis, such extrapolations are contained in the saturation model and in the CCFM amplitude; the use of the GRV gluon density, on the other hand, requires a momentum cutoff. In a final (and future) step one would need to find a QCD-based 'derivation' of the extrapolation from hard to soft physics.

Despite this encouraging success, several improvements in the theoretical part of our model should be made. First, since the cross section formula for $c\bar{c}g$ production has only been calculated in the leading log-M^2 approximation, an improvement which extends the applicability down to small-M^2 values would be very desirable. For consistency reasons, one then would need a NLO-calculation of $c\bar{c}$ production. Results of such a calculation would also allow to eliminate the cut on the transverse momentum of the final state gluon. Next, since the region of $x_{\mathbb{P}} > 0.02$ seems to require secondary exchanges, they should be modeled, in the framework of perturbative QCD, by $q\bar{q}$ exchange. Finally, our comparison with data indicates the need of $c\bar{c}gg$ final states: such an extension (at least in the leading log-M^2 approximation) should be fairly straightforward. A successful test of the two-gluon model in DIS Diffraction, apart form providing a description of charm or jet production at HERA, is also of general theoretical interest: the cross section formula for diffractive $q\bar{q} + ng$ production contains the perturbative triple Pomeron vertex which is expected to play a vital role in the unitarization of the BFKL approximation. It has been calculated both analytically and numerically, and these calculations can be tested experimentally in DIS diffraction dissociation.

References

[1] J. Bartels, H. Lotter, M. Wüsthoff, *Phys. Lett.* **B 379** (1996) 239, ERRATUM-ibid. **B 382** (1996) 449, hep-ph/9602363.

[2] N. Nikolaev, B. Zakharov, *Z. Phys.* **C 53** (1992) 331.

[3] E.Gotsman, E.Levin, U.Maor, *Nucl. Phys.* **B 493** (1997) 354.

[4] J. Bartels, H. Jung, M. Wusthoff, *Eur. Phys. J.* **C 11** (1999) 111, hep-ph/9903265.

[5] C. Adloff et al., *Eur. Phys. J.* **C 20** (2001) 29, hep-ex/0012051.

[6] H. Lotter, *Phys. Lett.* **B 406** (1997) 171, hep-ph/9612415.

[7] C. Adloff et al., *Phys. Lett.* **B 520** (2001) 191, hep-ex/0108047.

[8] ZEUS Collaboration, Diffractive $D^{*\pm}(2010)$ production in deep inelastic scattering at HERA, in *Proc. of the 30th International Conference on High Energy ICHEP 00* (Osaka, Japan, July, 2000), contributed paper 874.

[9] Partcile Data Group; C. Caso et al., *Eur. Phys. J.* **C 3** (1998) 1.

[10] H. Jung, *Comp. Phys. Comm.* **86** (1995) 147.

[11] H. Jung, *The RAPGAP Monte Carlo for Deep Inelastic Scattering, version 2.08*, Lund University, 2002, `http://www.quark.lu.se/~hannes/rapgap/`.

[12] T. Sjöstrand, *Comp. Phys. Comm.* **82** (1994) 74.

[13] T. Sjostrand et al., *Comput. Phys. Commun.* **135** (2001) 238, hep-ph/0010017.

[14] M. Glück, E. Reya, A. Vogt, *Z. Phys.* **C 67** (1995) 433.

[15] K. Golec-Biernat, M. Wüsthoff, *Phys. Rev.* **D 60** (1999) 114023.

[16] M. Ciafaloni, *Nucl. Phys.* **B 296** (1988) 49.

[17] S. Catani, F. Fiorani, G. Marchesini, *Phys. Lett.* **B 234** (1990) 339.

[18] S. Catani, F. Fiorani, G. Marchesini, *Nucl. Phys.* **B 336** (1990) 18.

[19] G. Marchesini, *Nucl. Phys.* **B 445** (1995) 49.

[20] H. Jung, G. Salam, *Eur. Phys. J.* **C 19** (2001) 351, hep-ph/0012143.

[21] H. Jung, *Phys. Rev.* **D 65** (2002) 034015, DESY-01-136, hep-ph/0110034.

[22] H. Jung, Unintegrated parton densities applied to heavy quark production in the CCFM approach, in *Proceedings of the Rinberg workshop on "New trends in HERA physics", Ringberg Castle, Tegernsee, Germany.* (2001), hep-ph/0109146.